

Communication

# Angle-Selective Photodetection in Ge/Si Quantum Dot Photodiodes Enhanced by Microstructured Hole Arrays

Andrew I. Yakimov <sup>1,\*</sup>, Victor V. Kirienko <sup>1</sup>, Aleksei A. Bloshkin <sup>1,2</sup>, Dmitrii E. Utkin <sup>1,2</sup>  
and Anatoly V. Dvurechenskii <sup>1,2</sup>

<sup>1</sup> Rzhanov Institute of Semiconductor Physics, Siberian Branch of the Russian Academy of Science, 630090 Novosibirsk, Russia; victor@isp.nsc.ru (V.V.K.); bloshkin@isp.nsc.ru (A.A.B.); utkinde@isp.nsc.ru (D.E.U.); dvurech@isp.nsc.ru (A.V.D.)

<sup>2</sup> Physical Department, Novosibirsk State University, 630090 Novosibirsk, Russia

\* Correspondence: yakimov@isp.nsc.ru

**Abstract:** We report on the near-infrared (NIR) photoresponse of a micropatterned Ge/Si quantum dot (QD) pin photodiode at different angles of radiation incidence. The photon-trapping hole array was etched through the n+-type top contact layer to reach the buried QDs. The normal-incidence responsivity was observed to be resonantly increased at wavelengths of 1.4, 1.7, and 1.9  $\mu\text{m}$  by factors of 40, 33, and 30, respectively, compared with the reference detector without holes. As the incident angle  $\theta$  increases, the resonance peaks are disappeared and at  $\theta > 40^\circ$  a new resonance with a  $25\times$  enhancement arises at a wavelength of 1.8  $\mu\text{m}$ . Simulation of the near-field intensity, Poynting vector distribution and wave polarization showed that at small  $\theta$ , the strong electric field is primarily localized under the air holes (1.4  $\mu\text{m}$ , TM mode) or between the holes (1.7 and 1.9  $\mu\text{m}$ , TE modes) inside the region occupied by QDs, resulting in the strong NIR photocurrent. At large  $\theta$ , the dominant resonance detected at 1.8  $\mu\text{m}$  is the result of coupling between the TE and TM modes and formation of a mixed near-field state.

**Keywords:** quantum dots; near-infrared photodetection; photon-trapping microstructures; telecom



**Citation:** Yakimov, A.I.; Kirienko, V.V.; Bloshkin, A.A.; Utkin, D.E.; Dvurechenskii, A.V. Angle-Selective Photodetection in Ge/Si Quantum Dot Photodiodes Enhanced by Microstructured Hole Arrays. *Photonics* **2023**, *10*, 764. <https://doi.org/10.3390/photonics10070764>

Received: 31 May 2023

Revised: 26 June 2023

Accepted: 29 June 2023

Published: 2 July 2023



**Copyright:** © 2023 by the authors. Licensee MDPI, Basel, Switzerland. This article is an open access article distributed under the terms and conditions of the Creative Commons Attribution (CC BY) license (<https://creativecommons.org/licenses/by/4.0/>).

## 1. Introduction

Photodetectors are optoelectronic devices with the ability to convert incident electromagnetic radiation into electric signals for further processing. Some recent progress towards height efficiency photodetectors can be found in [1–3]. Infrared (IR) photodetectors with low-dimensional nanostructures are widely used in applications, such as transmitting information, high-resolution imaging, atmospheric remote sensing, etc. [4–9]. Group-IV Ge/Si heterostructures can be monolithically integrated into silicon electronic chips providing a low cost and CMOS compatible photonics platform [10–13]. Nanostructured semiconductors based on assemblies of Ge/Si quantum dots (QDs) offer new opportunities for the development of costless and high-level integration infrared photodetectors. Among the various designs, Ge/Si QD photodiodes integrated with photon-trapping hole array structures are highlighted. However, Ge/Si QD IR photodetectors (QDIPs) are not used traditionally due to its weak absorption coefficient caused by low density of states associated with QDs [14–17], spatial separation of the charge carriers by the heterointerface [18–21] and comparatively large effective mass. Furthermore, although recently there has been significant progress in the development of approaches to the creation of high-performance QDIPs, it still needs to make further improvements. Recent works have shown that using all-dielectric photon-trapping hole array structures could be regarded as an effective approach to enhance the performance of Si-based photodiodes with a thin absorption region due to light trapping and excitation of in-plane guiding modes [22–29].

Vertical Ge/Si QD pin photodiodes grown on a silicon-on-insulator (SOI) substrate and integrated with photon-trapping hole arrays have been demonstrated in [30,31]. By mi-

cro patterning QDIPs, we managed to redirect normal incident light laterally along the planes of the dots. The research results demonstrated that this approach can realize the peak photoresponse of the Ge/Si QDIPs in the NIR wavelength range and yield up to  $(30\text{--}50)\times$  enhanced responsivity than that without the microhole structure. Light trapping due to excitation of in-plane propagating modes and reduced reflection is a major cause of the photocurrent enhancement [31]. Usually, the studies of light-trapping-enhanced photodetection are restricted to normal incidence and little is known about the dependence of the detector performance on the incident angle of the light source. However, it could be very useful in many applications, such as high response angle-sensing photodetection, solar energy conversion, laser beacon tracking, lensless imaging, etc. [32–37]. In the present work, we study the angular-dependent photodetection in Ge/Si QDIPs containing microhole arrays on their surface. We found that the responsivity enhancement spectra strongly depend on the angle of incidence, indicating the angle selective behavior of the device.

### 2. Materials and Methods

A schematic of our QD pin photodiode with array of holes is shown in Figure 1a. A detailed description of the electronic structure of Ge/Si QDs and the growth conditions, such as growth temperature and growth rate has been reported earlier [21,30]. A brief overview of the QDIP fabrication is summarized as below:

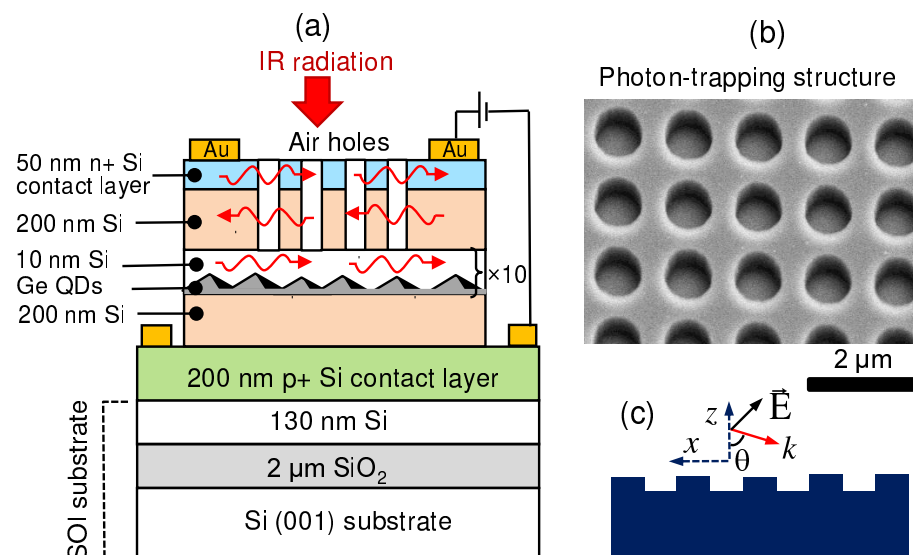


**Figure 1.** (a) A cross sectional view of a pin QDIP photodiode on a SOI wafer with the holes on its surface. (b) Tilted view SEM image of the 2D hole array (photon-trapping structure). The hole diameter is 850 nm and lattice periodicity is 1300 nm. The hole depth is 250 nm. (c) The geometry of the angular-resolved experiments.

The QDIP sample was grown on a (001)-oriented SOI wafer with a 110 nm top silicon film and 2 μm buried silicon oxide using a Riber SIVA-21 molecular beam epitaxy system. A 200 nm B-doped p-type Si bottom contact layer ( $5 \times 10^{18} \text{ cm}^{-3}$ ) is first fabricated, followed by the growth of a 200 nm undoped Si buffer layer. Ten layers Ge QD active region was then grown. QDs have a hut-like shape with a lateral size of 10 nm and a height of about 1 nm. The surface density of QDs is  $5 \times 10^{11} \text{ cm}^{-2}$ . A 10 nm Si barrier layer was grown between two adjacent QD layers. The structure was cover by a 200 nm top Si buffer layer, followed by the Sb doped 50 nm thick  $n^+$  top contacting layer ( $\sim 10^{19} \text{ cm}^{-3}$ ).

After the growth, the photon-trapping hole array with a square lattice symmetry was fabricated on top of the diode by electron-beam lithography and reactive ion etching of Si layers through a metallic mask. The array period is 1300 nm with 850 nm circular etched holes. Note that the dimensions of QDs are many orders of magnitude smaller than the hole diameter and period. The scanning electron microscopy (SEM) image of the sample

is shown in Figure 1b. The holes were etched to 250 nm depth to reach the buried QD layers. The selected depth corresponds to the one at which the maximum responsivity enhancement was previously observed [31]. Microholes promote lateral propagating modes. By changing the depth of the hole, it is possible to change the vertical position of the maximum intensity of the lateral modes through the detector. The use of a light-trapping structure with holes passing through the QD absorber is advantageous for optical field confinement within the QD active region, but at the expense of reducing the number of QDs, which leads to less absorption. The optimum hole depth appears as a result of trade-off between the amount of absorbing QD layers remaining after etching of holes and enhanced light intensity in the region of QDs due to generation of guiding collective modes [31]. The light-trapping structure has covered about 70% of the light absorption area. A control sample without holes was also fabricated for the comparison of device performance. Its photocurrent was used as a reference with that of a patterned device. Both flat and microstructured samples were taken from a single die of the same wafer right next to each other. Discrete devices were fabricated by standard processing technique. The diode structure was a 700  $\mu\text{m}$  diameter circular mesa with a 500  $\mu\text{m}$  diameter open aperture and AuTi contact rings.

The photodiode response was characterized at room temperature using a Bruker Vertex 70 Fourier spectrometer with a spectral resolution of 30  $\text{cm}^{-1}$  along and a Stanford Research SR570 low-noise current. A halogen lamp was used as a source of radiation. The photocurrent spectra were calibrated with a deuterated L-alanine doped triglycine sulfate detector. The responsivity was determined by illuminating the samples with the InGaAsP LEDs (Roithner Laser Technik), which were emitting at 1.3 and 1.55  $\mu\text{m}$ . The samples under test are reverse-biased at  $U = 0$  to 2.5 V and the wavelength of the incident light was varied from 0.8 to 2.3  $\mu\text{m}$ . Angular photoresponse characterization was used to obtain insights into the optical resonant features. For this purpose, we shed the global light to the top of the device at a fixed position with the device varied at different incident angles by using the electronically controlled rotational platform. The light was linearly polarized orthogonal to the axis of rotation (Figure 1c). The incidence angle was varied from  $\theta = 0^\circ$  to  $60^\circ$  with the accuracy of  $1^\circ$ .

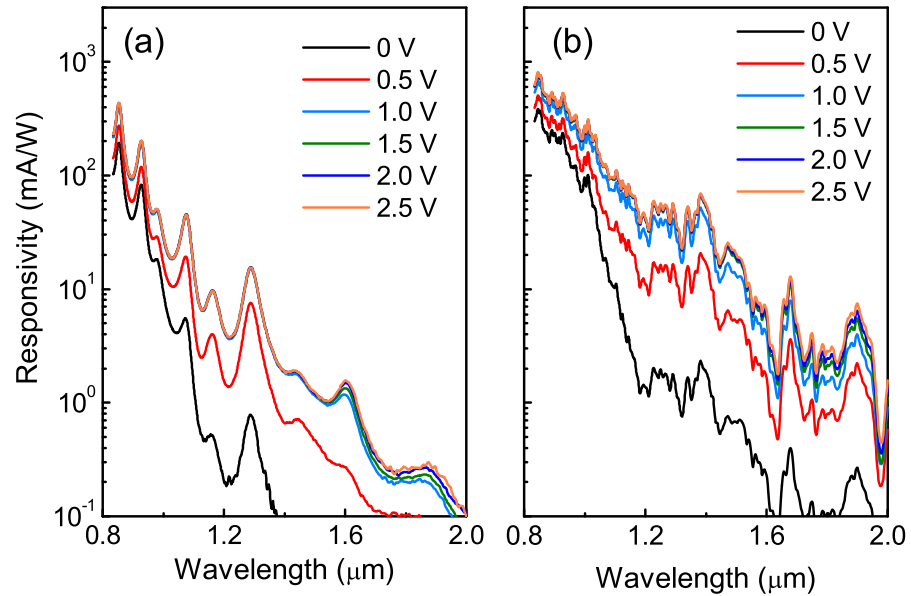
### 3. Results and Discussion

Figure 2 depicts the measured normal-incidence ( $\theta = 0^\circ$ ) responsivity spectra of the detectors with and without photon-trapping holes with different reverse bias voltages. The responsivity of both devices rapidly increases with the bias voltage and saturates at  $U \geq 1$  V. The weak dependence of the photocurrent on the bias indicates efficient collection of photogenerated carriers. The spectral response of the unpatterned detector without a texture pit is undulating. The light in the detector active region experiences a strong reflection at air/Si and Si/SiO<sub>2</sub> interfaces of the SOI substrate, creating a resonant cavity. Large responsivity oscillations observed on the spectra of the control detector is a result of the strong vertical Fabry–Pérot resonances due to interference of the waves reflected at these interfaces [31,38]. The micropatterned QDIP with a textured surface has much weaker vertical resonances, which suggests a successful transformation of the initial incident vertical plane wave into an ensemble of modes propagating in the lateral direction. Waveguiding of the light enlarges the effective optical interaction length and results in photocurrent enhancement. We define the photocurrent enhancement ratio  $K$  as follows

$$K = \frac{I_{PT}}{I_{ref}}, \quad (1)$$

where  $I_{PT}$  is the photocurrent of the photon-trapping QDIP and  $I_{ref}$  is the photocurrent of the control sample with a flat surface. The photocurrent enhancement at 2 V is plotted in Figure 3. Compared with the conventional QDIP without holes, the responsivity of photon-trapping detector has a broadband (10–15) $\times$  oscillating improvement, which allows the operation wavelength extended to about 2.0  $\mu\text{m}$  with the responsivity of about 10 mA/W.

Similar broadband absorption enhancement has been previously observed in high-speed Si-based and InAsSb-GaSb photodetectors [23–29,39] and attributed to the generation of the waves with the Poynting vector directed horizontally from the holes into adjacent semiconductor material. Photons are diffracted by the micropatterned surface and maintain in-plane momentum by waveguiding between the buried reflecting oxide layer and the air–Si surface [38].



**Figure 2.** Plots of responsivity vs. wavelength of the Ge/Si QDIPs (a) without and (b) with photon-trapping hole array at different reverse bias. The spectra were measured at normal incident non-polarized radiation.

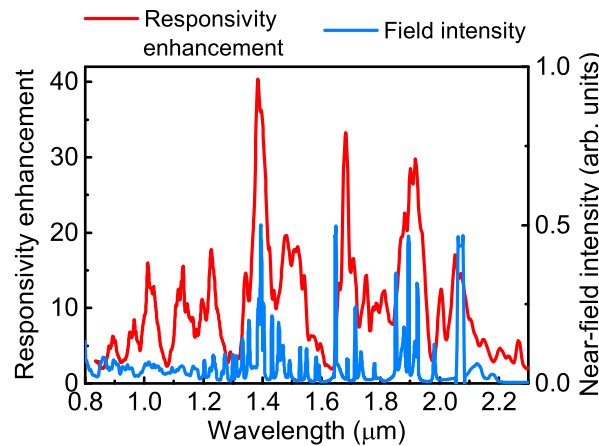


**Figure 3.** Spectral characteristics of (left scale) the measured photocurrent enhancement and (right scale) the calculated integrated intensity of the near field over the QD active region at normal incident radiation. The hole depth is 250 nm.

In addition to a wide enhancement band, the sharp peaks with the amplitude of 40, 33, and 30 are found at wavelengths of 1.4, 1.7, and 1.9  $\mu\text{m}$ , respectively. An external quantum efficiency ( $\eta$ ) can be calculated using the relation

$$\eta = \frac{hc R}{e \lambda}, \tag{2}$$

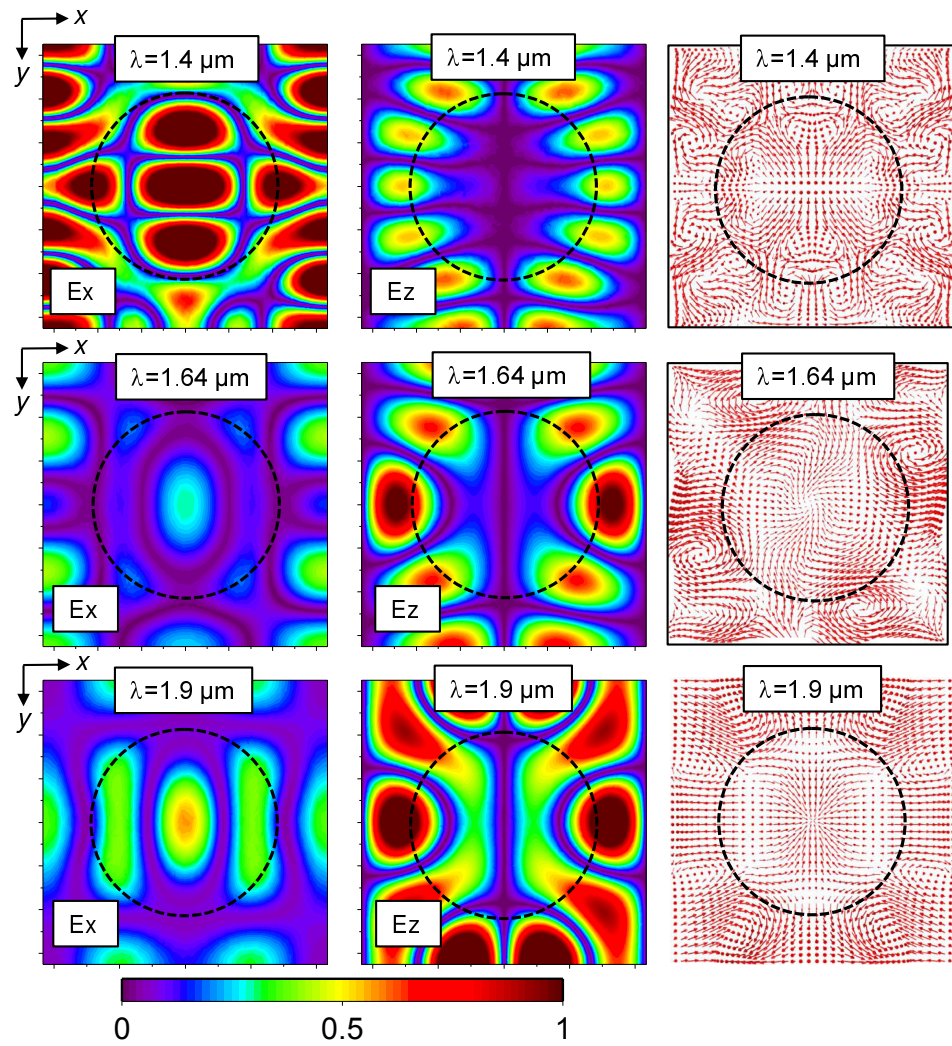
in which  $h$ ,  $c$ ,  $R$ ,  $e$ , and  $\lambda$  are the Plank constant, light velocity, elementary charge, and illumination wavelength, respectively. At  $U \geq 1$  V, the quantum efficiency of the light-trapping

detector was found to be 6.7, 0.96, and 0.52% at peak wavelength  $\lambda = 1.4, 1.7,$  and  $1.9 \mu\text{m}$ , respectively. Since the resonance enhancement maxima occur at  $\lambda > p$ , where  $p = 1.3 \mu\text{m}$  is the period of the hole array, one can suppose that a series of resonant features corresponds to the excitation of the Bloch modes of the photonic crystal [22,40–43].

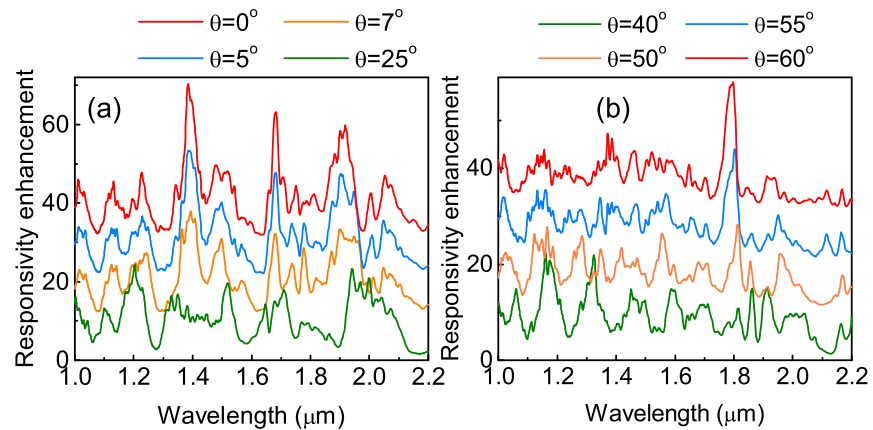
To clarify the character of electromagnetic excitations responsible for an increase in the photocurrent, we analyzed the spatial distribution of the near field components and Poynting vectors in the QDIP shown in Figure 1. The method of the calculation is similar to that reported in [30,44]. The electromagnetic field appearing in the PC was simulated by the finite element method with the Comsol Multiphysics simulation software. To exclude non-physical reflections of a light wave, perfect matched layer boundary conditions were used on the upper and lower boundaries of the domain. The polarization of incident radiation was chosen circular or linear. Figure 3 shows the integrated near-field intensity over the QD active region, i.e.,  $\int_V |E|^2 dV$ , where  $V$  indicates volume integral over the QD region. One can find that the spectrum of  $\int_V |E|^2 dV$  closely resembles the enhancement factor spectrum. The experimental photocurrent enhancement in Figure 3 shows a broader spectral width than the simulated peaks. This might be due both to the scattering of photo-excited charge carriers by the fluctuating potential of charged walls of holes and to the fluctuations of the sizes, shapes, and period of the holes.

Figure 4 demonstrates that the periodic hole array acts like a conventional grating coupler and supports a set of modes in both vertical and lateral directions. The lateral waves represent the guided resonance modes [22]. They travel exactly along the QD layers and can efficiently interact with the dots and increase the QDIP photoresponse. At the wavelength of  $1.4 \mu\text{m}$ , the dominant field component is in-plane  $E_x$  component concentrated both under the holes and between the holes. The  $1.4 \mu\text{m}$ -wavelength resonance polarized perpendicular to the axis of the holes corresponds to the TM mode of the photonic crystal [45]. At longer wavelengths, the vertical  $E_z$  field component primarily localized between the holes becomes a dominant component of the guided modes. Therefore, the long-wave ( $1.7$  and  $1.9 \mu\text{m}$ ) resonances with the electric field vector parallel to the hole axis can be classified as the TE modes [45].

Figure 5 shows the responsivity enhancement spectra of the light-trapping enhanced QDIP at different plane wave incident angles. The broadband oscillating background does not depend on light incident angle. Like the resonance peaks found in the responsivity of resonant-cavity-enhanced detectors [32], the peak photoresponse of the light-trapping QDIP is very sensitive to  $\theta$ . With  $\theta$  increasing, the resonant features become less pronounced and disappeared at  $\theta \simeq 10^\circ$ . At  $\theta > 40^\circ$ , a new resonance with a  $25\times$  enhancement emerges at a wavelength of  $1.8 \mu\text{m}$ . Figure 6 plots the simulated near field components distribution at  $\theta = 60^\circ$  at excitation wavelengths of  $1.4$  and  $1.8 \mu\text{m}$ . In agreement with the experimental observation, the optical field at  $1.4 \mu\text{m}$  and at large  $\theta$  is very weak. The dominant resonance with high field components  $|E_x|$  and  $|E_z|$  comparable in intensity is excited at  $1.8 \mu\text{m}$ . The  $E_x$  field component is mainly localized under the hole, whereas  $E_z$  is concentrated around the hole. The Poynting vector is directed laterally, which means that the NIR light spread in the lateral direction and then remains confined in Ge/Si QD layers until it becomes absorbed by the dots. Since both the  $x$ - and  $z$ -polarized waves are present, we may conclude that the resonance detected at  $1.8 \mu\text{m}$  is a result of coupling between the TE and TM modes and formation of a mixed near-field state.



**Figure 4.** Color maps of the spatial distribution of the near-field components  $|E_x|$  and  $|E_z|$  and the Poynting vectors at resonant wavelengths in the  $(x, y)$  plane in a micropatterned photodetector. The hole array parameters are  $d = 850$  nm (hole diameter) and  $p = 1300$  nm (hole period). The hole depth is 250 nm. The data were taken at the distance of 300 nm below the device surface. i.e., in the middle of the QD active region. The dashed lines indicate the boundaries of the holes. The arrows represent the energy flux direction. The structure was illuminated at  $\theta = 0^\circ$  from the front side with a plane-wave light polarized in the  $x$  direction.



**Figure 5.** Responsivity enhancement ratio spectra as a function of incident angle at (a) small and (b) large  $\theta$  for light polarized orthogonal to the axis of rotation. The spectra are vertically offset by 10 units.

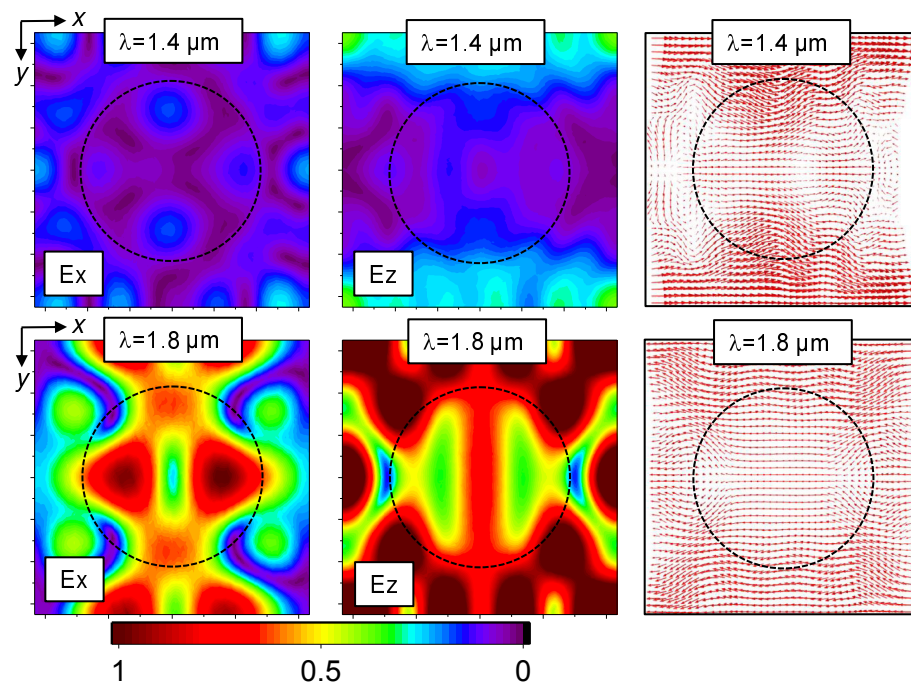


**Figure 6.** Simulated lateral distribution maps of the electric field components  $|E_x|$  and  $|E_z|$  and the Poynting vector in the  $(x, y)$  plane at  $\lambda = 1.4$  and  $1.8 \mu\text{m}$ . The data were taken at the distance of  $300 \text{ nm}$  below the device surface. i.e., in the middle of the QD active region. The dashed lines indicate the boundaries of the holes. The structure was illuminated at  $\theta = 60^\circ$  from the front side with a plane-wave light polarized in the  $x$  direction.

#### 4. Conclusions

In summary, we study the angular-dependent photodetection in a Ge/Si QDIP containing microhole arrays on its surface. The light-trapping holes enhance the absorption of Ge quantum dots and extend the operational wavelength of the photodiode to  $2 \mu\text{m}$  with the responsivity of about  $10 \text{ mA/W}$ . This represents (30–40) fold increased efficiency compared to conventional flat QDIP without holes. The enhancement spectrum consists of both the broad band and the resonance peaks. We found that the resonance features strongly depend on the angle of incidence, indicating the angle-selective behavior of the device.

**Author Contributions:** Conceptualization, A.I.Y.; methodology, V.V.K. and D.E.U.; software, A.A.B.; investigation, A.I.Y. and V.V.K.; writing—original draft preparation, A.I.Y.; writing—review and editing, V.V.K., A.V.D. and D.E.U.; visualization, D.E.U.; supervision, A.V.D.; funding acquisition, A.V.D. All authors have read and agreed to the published version of the manuscript.

**Funding:** This research was funded by Russian Science Foundation (grant 19-12-00070-II).

**Institutional Review Board Statement:** Not applicable.

**Informed Consent Statement:** Not applicable.

**Data Availability Statement:** Data are contained within the article.

**Acknowledgments:** We thank the Multiple-access Center “Nanostructures” at Rzhanov Institute of Semiconductor Physics for the provision of technological and diagnostic equipment. Electron lithography and SEM experiments were performed at the Analytical and Technological Research Center in the Physical Department of Novosibirsk State University.

**Conflicts of Interest:** The authors declare no conflict of interest.

## References

1. Li, W.G.; Wang, X.D.; Liao, J.F.; Jiang, Y.; Kuang, D.B. Enhanced on-off ratio photodetectors based on lead-free Cs<sub>3</sub>Bi<sub>2</sub>I<sub>9</sub> single crystal thin films. *Adv. Funct. Mater.* **2020**, *30*, 1909701. [[CrossRef](#)]
2. Song, W.; Chen, J.; Li, Z.; Fang, X. Self-powered MXene/GaN van der Waals heterojunction ultraviolet photodiodes with superhigh efficiency and stable current outputs. *Adv. Mater.* **2021**, *33*, 2101059. [[CrossRef](#)]
3. Han, S.; Quan, J.; Wang, D.; Li, H.; Liu, X.; Xu, J.; Zhang, Y.; Li, Z.; Wu, L.; Fang, X. Anisotropic growth of centimeter-size CsCu<sub>2</sub>I<sub>3</sub> single crystals with ultra-low trap density for aspect-ratio-dependent photodetectors. *Adv. Sci.* **2023**, *10*, 2206417. [[CrossRef](#)] [[PubMed](#)]
4. Tong, J.; Suo, F.; Ma, J.; Tobing, L.; Qian, L.; Zhang, D. Surface plasmon enhanced infrared photodetection. *Opto-Electron. Adv.* **2019**, *2*, 180026. [[CrossRef](#)]
5. Patra, A.; Rout, C.S. Self-Assembled Quantum Dot Photodetector: A Pathbreaker in the Field of Optoelectronics. In *Quantum Dot Photodetectors*; Tong, X., Wu, J., Wang, Z.M., Eds.; Springer: Cham, Switzerland, 2021; pp. 289–305.
6. Hu, X.; Wu, J.; Wu, M.; Hu, J. Recent developments of infrared photodetectors with low-dimensional inorganic nanostructures. *Nano Res.* **2022**, *15*, 805–817. [[CrossRef](#)]
7. Hao, Q.; Zhao, X.; Tang, X.; Chen, M. The historical development of infrared photodetection based on intraband transitions. *Materials* **2023**, *16*, 1562. [[CrossRef](#)]
8. Guo, H.; Qi, W. New materials and designs for 2D-based infrared photodetectors. *Nano Res.* **2023**, *16*, 3074–3103. [[CrossRef](#)]
9. Yan, N.; Qiu, Y.; He, X.; Tang, X.; Hao, Q.; Chen, M. Plasmonic enhanced nanocrystal infrared photodetectors. *Materials* **2023**, *16*, 3216. [[CrossRef](#)] [[PubMed](#)]
10. Paul, D. Si/SiGe heterostructures: From material and physics to devices and circuits. *Semicond. Sci. Technol.* **2004**, *19*, R75–R108. [[CrossRef](#)]
11. Michel, J.; Liu, J.; Kimerling, L.C. High-performance Ge-on-Si photodetectors. *Nat. Photonics* **2010**, *4*, 527–534. [[CrossRef](#)]
12. Sood, A.K.; Zeller, J.W.; Richwine, R.A.; Puri, Y.R.; Efsathiadis, H.; Haldar, P.; Dhar, N.K.; Polla, D.L. SiGe-based visible-NIR photodetector technology for optoelectronic applications. In *Advances in Optical Fiber Technology: Fundamental Optical Phenomena and Applications*; Yasin, M., Arof, H., Harun, S.W., Eds.; Intech: Rijeka, Croatia, 2015; pp. 315–362.
13. Douhan, R.; Lozovoy, K.; Kokhanenko, A.; Deeb, H.; Dirko, V.; Khomyakova, K. Recent advances in Si-compatible nanostructured photodetectors. *Technologies* **2023**, *11*, 17. [[CrossRef](#)]
14. Tong, S.; Liu, J.; Wang, J.; Wang, K. Normal-incidence Ge quantum-dot photodetectors at 1.5 μm based on Si substrate. *Appl. Phys. Lett.* **2002**, *80*, 1189–1191. [[CrossRef](#)]
15. Alguno, A.; Usami, N.; Ujihara, T.; Fujiwara, K.; Sazaki, G.; Nakajima, K.; Shiraki, Y. Enhanced quantum efficiency of solar cells with self-assembled Ge dots stacked in multilayer structure. *Appl. Phys. Lett.* **2003**, *83*, 1258–1260. [[CrossRef](#)]
16. Elfving, A.; Hansson, G.; Ni, W.X. SiGe (Ge-dot) heterojunction phototransistors for efficient light detection at 1.3–1.55 μm. *Physica E* **2003**, *16*, 528–532. [[CrossRef](#)]
17. Yakimov, A.I.; Kirienko, V.V.; Armbrister, V.A.; Bloshkin, A.A.; Dvurechenskii, A.V. Photoconductive gain and quantum efficiency of remotely doped Ge/Si quantum dot photodetectors. *Mater. Res. Express* **2016**, *3*, 105032. [[CrossRef](#)]
18. Brunner, K. Si/Ge nanostructures. *Rep. Prog. Phys.* **2002**, *65*, 27–72. [[CrossRef](#)]
19. Schmidt, O.G.; Eberl, K.; Rau, Y. Strain and band-edge alignment in single and multiple layers of self-assembled Ge/Si and GeSi/Si islands. *Phys. Rev. B* **2000**, *62*, 16715–16720. [[CrossRef](#)]
20. Grützmacher, D.; Fromherz, T.; Dais, C.; Stangl, J.; Müller, E.; Ekinci, Y.; Solak, H.; Sigg, H.; Lechner, R.; Wintersberger, E.; et al. Three-Dimensional Si/Ge Quantum Dot Crystals. *Nano Lett.* **2007**, *7*, 3150–3156. [[CrossRef](#)] [[PubMed](#)]
21. Yakimov, A.I.; Kirienko, V.V.; Bloshkin, A.A.; Dvurechenskii, A.V.; Utkin, D.E. Near-infrared photoresponse in Ge/Si quantum dots enhanced by localized surface plasmons supported by aluminium nanodisks. *J. Appl. Phys.* **2020**, *128*, 143101. [[CrossRef](#)]
22. Donnelly, J.L.; Sturmberg, B.C.; Dossou, K.B.; Botten, L.C.; Asatryan, A.A.; Poulton, C.G.; McPhedran, R.C.; de Sterke, M. Mode-based analysis of silicon nanohole arrays for photovoltaic applications. *Opt. Express* **2014**, *22*, A1343–A1354. [[CrossRef](#)]
23. Gao, Y.; Cansizoglu, H.; Polat, K.G.; Ghandiparsi, S.; Kaya, A.; Mamtaz, H.H.; Mayet, A.S.; Wang, Y.; Zhang, X.; Yamada, T.; et al. Photon-trapping microstructures enable high-speed high-efficiency silicon photodiodes. *Nat. Photonics* **2017**, *11*, 301–309. [[CrossRef](#)]
24. Cansizoglu, H.; Bartolo-Perez, C.; Gao, Y.; Ponizovskaya Devine, E.; Ghandiparsi, S.; Polat, K.G.; Mamtaz, H.H.; Yamada, T.; Elrefaie, A.F.; Wang, S.Y.; et al. Surface-illuminated photon-trapping high-speed Ge-on-Si photodiodes with improved efficiency up to 1700 nm. *Photonics Res.* **2018**, *6*, 734–742. [[CrossRef](#)]
25. Ghandiparsi, S.; Elrefaie, A.F.; Mayet, A.S.; Landolsi, T.; Bartolo-Perez, C.; Cansizoglu, H.; Gao, Y.; Mamtaz, H.H.; Golgir, H.R.; Ponizovskaya Devine, E.; et al. High-speed high-efficiency pin photodiodes for short-reach optical interconnects in data centers. *IEEE J. Light. Technol.* **2019**, *37*, 5748–5755. [[CrossRef](#)]
26. Zhou, H.; Xu, S.; Lin, Y.; Huang, Y.C.; Son, B.; Chen, Q.; Guo, X.; Lee, K.H.; Gon, S.C.K.; Gong, X.; et al. High-efficiency GeSn/Si multiple-quantum-well photodetectors with photon-trapping microstructures operating at 2 μm. *Opt. Express* **2020**, *28*, 10280–10293. [[CrossRef](#)] [[PubMed](#)]
27. Cansizoglu, H.; Ponizovskaya Devine, E.; Gao, Y.; Ghandiparsi, S.; Yamada, T.; Elrefaie, A.F.; Wang, S.Y.; Islam, M.S. A new paradigm in high-speed and high-efficiency silicon photodiodes for communication – Part I: Enhancing photon-material interaction via low-dimensional structures. *IEEE Trans. Electron Devices* **2018**, *65*, 372–381. [[CrossRef](#)]

28. Yamada, T.; Ponizovskaya Devine, E.; Ghandiparsi, S.; Bartolo-Perez, C.; Mayet, A.S.; Cansizoglu, H.; Gao, Y.; Ahamed, A.; Wang, S.Y.; Islam, M.S. Modeling of nanohole silicon pin/nip photodetectors: Steady state and transient characteristics. *Nanotechnology* **2021**, *32*, 365201. [[CrossRef](#)] [[PubMed](#)]
29. Bartolo-Perez, C.; Chandiparsi, S.; Mayet, A.S.; Cansizoglu, H.; Gao, Y.; Qarony, W.; Ahamed, A.; Wang, S.Y.; Cherry, S.R.; Islam, M.S.; et al. Avalanche photodetectors with photon trapping structures for biomedical imaging applications. *Opt. Express* **2021**, *29*, 19024–19033. [[CrossRef](#)]
30. Yakimov, A.I.; Kirienko, V.V.; Bloshkin, A.A.; Utkin, D.E.; Dvurechenskii, A.V. Near-infrared photoresponse in Ge/Si quantum dots enhanced by photon-trapping hole arrays. *Nanomaterials* **2021**, *11*, 2302. [[CrossRef](#)]
31. Yakimov, A.I.; Kirienko, V.V.; Utkin, D.E.; Dvurechenskii, A.V. Light-trapping-enhanced photodetection in Ge/Si quantum dot photodiodes containing microhole arrays with different hole depths. *Nanomaterials* **2022**, *12*, 2993. [[CrossRef](#)]
32. Ünlü, M.S.; Strite, S. Resonant cavity enhanced photonic devices. *J. Appl. Phys.* **1995**, *78*, 607–639. [[CrossRef](#)]
33. Shen, Y.; Ye, D.; Celanovic, I.; Johnson, S.G.; Joannopoulos, J.D.; Soljačić, M.S. Optical broadband angular selectivity. *Science* **2014**, *343*, 1499–1501. [[CrossRef](#)]
34. Kemsri, T.; Gu, G.; Zhang, Y.; Lan, X.; Zhang, H.; Tice, J.; Lu, X. Angular-dependent photodetection enhancement by a metallic circular disk optical antenna. *AIP Adv.* **2017**, *7*, 025013. [[CrossRef](#)]
35. Yi, S.; Zhou, M.; Yu, Z.; Fan, P.; Behdad, N.; Lin, D.; Wang, K.X.; Fan, S.; Brongersma, M. Subwavelength angle-sensing photodetectors inspired by directional hearing in small animals. *Nat. Nanotechnol.* **2018**, *13*, 1143–1147. [[CrossRef](#)]
36. Nagarajan, A.; Hara, S.; Satoh, H.; Panchanathan, A.P.; Inokawa, H. Angular selectivity of SOI photodiode with surface plasmon antenna. *IEICE Electron. Express* **2020**, *17*, 1–6. [[CrossRef](#)]
37. Huang, C.H.; Wu, C.H.; Bikbaev, R.G.; Ye, M.J.; Chen, C.W.; Wang, T.J.; Timofeev, I.V.; Lee, W.; Chen, K.P. Wavelength- and angle-selective photodetectors enabled by graphene hot electrons with Tamm plasmon polaritons. *Nanomaterials* **2023**, *13*, 693. [[CrossRef](#)] [[PubMed](#)]
38. Zang, K.; Jiang, X.; Huo, Y.; Ding, X.; Morea, M.; Chen, X.; Lu, C.Y.; Ma, J.; Zhou, M.; Xia, Z.; et al. Silicon single-photon avalanche diodes with nanostructured light trapping. *Nat. Commun.* **2017**, *8*, 628. [[CrossRef](#)] [[PubMed](#)]
39. Suo, F.; Tong, J.; Zhang, D.H. Photon-trapping array for enhanced midwave infrared photoresponse. *J. Phys. D Appl. Phys.* **2021**, *54*, 505105. [[CrossRef](#)]
40. Baba, T. Slow light in photonic crystals. *Nat. Photonics* **2008**, *2*, 465–473. [[CrossRef](#)]
41. Duché, D.; Escoubas, L.; Simon, J.J.; Torchio, P.; Vervisch, W.; Flory, F. Slow Bloch modes for enhancing the absorption of light in thin films for photovoltaic cells. *Appl. Phys. Lett.* **2008**, *92*, 193310. [[CrossRef](#)]
42. Sturmberg, B.C.; Dossou, K.B.; Botten, L.C.; Asatryan, A.A.; Poulton, C.G.; de Sterke, M.; McPhedran, R.C. Modal analysis of enhanced absorption in silicon nanowire arrays. *Opt. Express* **2011**, *19*, A1067–A1081. [[CrossRef](#)] [[PubMed](#)]
43. Gomard, G.; Peretti, R.; Callard, S.; Meng, X.; Artinyan, R.; Deschamps, T.; i Cabarrocas, P.R.; Drouard, E.; Seassal, C. Blue light absorption enhancement based on vertically channeling modes in nano-hole arrays. *Appl. Phys. Lett.* **2014**, *104*, 051119. [[CrossRef](#)]
44. Yakimov, A.I.; Bloshkin, A.A.; Dvurechenskii, A.V. Tailoring the optical field enhancement in Si-based structures covered by nanohole arrays in gold films for near-infrared photodetection. *Photonics Nanostruct.* **2020**, *40*, 100790. [[CrossRef](#)]
45. Joannopoulos, J.D.; Johnson, S.G.; Winn, J.N.; Meade, R.D. *Photonic Crystals: Molding the Flow of Light*; Princeton University Press: Princeton, NJ, USA; Oxford, UK, 2008.

**Disclaimer/Publisher’s Note:** The statements, opinions and data contained in all publications are solely those of the individual author(s) and contributor(s) and not of MDPI and/or the editor(s). MDPI and/or the editor(s) disclaim responsibility for any injury to people or property resulting from any ideas, methods, instructions or products referred to in the content.